Non-adiabatic Molecular Dynamics Study of the Relaxation Pathways of Photoexcited Cyclooctatetraene

Huajing Song,[*,†] Yeonsig Nam,[‡] Daniel Keefer,[‡] Marco Garavelli,[¶] Shaul Mukamel,[‡,§] and Sergei Tretiak[*,†,‖]

†*Physics and Chemistry of Materials, Theoretical Division, Los Alamos National Laboratory, Los Alamos, New Mexico, 87545, USA*

‡*Department of Chemistry, University of California, Irvine, CA 92697, USA*

¶*Department of Industrial Chemistry, "T. Montanari", Università degli Studi di Bologna, Viale del Risorgimento, 4, 40136 Bologna, Italy*

§*Department of Physics and Astronomy, University of California, Irvine, CA 92697, USA*

‖*Center for Integrated Nanotechnologies, Los Alamos National Laboratory, Los Alamos, New Mexico 87545, USA*

E-mail: songhw@lanl.gov; serg@lanl.gov

Abstract

In the current study, we present non-adiabatic (NAMD) and adiabatic molecular dynamics simulations of the transition-state dynamics of photoexcited cyclooctatetraene (COT). The equilibrium state structure and absorption spectra are analyzed using the semiempirical Austin Model 1 potential. The following NAMD simulation are obtained by a surface-hopping algorithm. We analyzed in detail an active excited to ground state relaxation pathway accompanied with a $S_2/S_3(D_{2d}) \rightarrow S_1(D_{8h}) \rightarrow S_0(D_{4h}) \rightarrow S_0(D_{2d})$ double-bond shifting mechanism. The simulated excitation lifetime is in good agreement with experiment. The first excited singlet state S_1 plays a crucial role in the photochemistry. The obtained critical molecular conformations, energy barrier, and transition state lifetime results will provide a basis for further investigations of the bond order inversion and photo-switching process of COT.

Photo-switches are molecular systems that change their geometry and properties upon optical excitation[1,2] and may find applications in biology, chemistry and nanotechnology. Photoisomerization is a typical example of such switching,[3–5] e.g., observed in rhodopson, which constitutes an initial step in the human and animal vision.[6,7] Cyclooctatetraene (COT) is a conjugated cyclic 4n π-electrons system that gains aromaticity with a planar structure with equal C-C bond lengths in the first singlet excited state S_1, but is non-aromatic in higher excited-state $S_{n>1}$ and in the ground state (S_0), where it assumes a non-planar boat-like structure with localized single and double C-C bonds. Upon UV excitation, COT's non-radiative decay via a polyradical S_1/S_0 conical intersection also promotes a bond order inversion in the ground state, which also know as double-bond shift (i.e., a π-skeletal rearrangement).[8] This process occurs when the π-electrons "migrate" within the octagonal perimeter resulting in a site exchange between singly and doubly bonded carbon atoms. Such photoinduced double-bond shifting reaction may be exploited to design photochemically driven molecular switches,[1] where an "on-state" is characterized by "through-conjugation"

between the π-donor and π-acceptor substituents, whereas an "off-state", refers to a suppression of this through-conjugation. COT thus appears as a particularly suitable candidate for studying both the double-bond shifting and the non-aromatic (S_0)/aromatic (S_1) photoswitching process.[8–11]

The excited-state relaxation pathway plays a key role in its photochemistry. Using complete active space self-consistent field (CASSCF) and CAS second-order perturbation theory (CASPT2) with minimum energy path (MEP) method, Garavelli et al.[8] have identified some possible pathways for the formation of photochemical structures of COT. Proposed mechanism describes that the photon initially excites COT to the bright (i.e., optically allowed) S_2 state, which decays then efficiently to the dark (i.e., optically forbidden) S_1 state. The following nonadiabatic transitions the ground state S_0 appear to be controlled by two different tetraradical-type conical intersection, which are accessed by S_1 excited-state reaction paths. The higher-energy conical intersection configuration (CI_{st}) is featured by a triangular -$(CH)_3$- kink, and the lowest energy conical intersection has a folded quasi-tetraradical structure CI_b. Further relaxation on the S_0 potential-energy surfaces results in different product channels. In a series of recent studies, Takayanagi et al.[10,12,13] have applied the ground state *ab initio* MD to study the photoionization of COT. However, due to the lack of appropriate excited-state potential and conical intersection dynamics information, the timescale obtained from their reduced-dimensionality quantum dynamics calculations and the on-the-fly classical dynamics calculations is too short compared to the experiment. By thermal fluctuations, only one (or two) relaxation pathways would dominate the excited-state dynamic at finite temperatures. Here we apply a non-adiabatic molecular dynamic (NAMD) simulation method to study the excited-state dynamics and determine the relaxation pathways of photoexcited COT.

The excited state molecular dynamics of COT is calculated using Tully's fewest switches surface hopping (FSSH)[14] approach combined with empirical decoherence corrections[15] and trivial crossing tracking[16] algorithms as implemented into the Non-adiabatic Excited state

Molecular Dynamics (NEXMD) package.[17–19] By applying the collective electron oscillator method[20] with the semiempirical Austin Model 1 (AM1) Hamiltonian[21] at the configuration interaction singles (CIS)[22] level, the NEXMD can routinely handle the NAMD simulation up to 20 picoseconds (ps). This package has been successfully applied to the modeling of photoinduced processes in many other molecular systems.[23–25]

Our simulations find that COT has non-aromatic equilibrium boat-shaped structures in the ground state and higher excited-state S_n (n = 2 or 3), and planar antiaromatic metastable structures in the ground state. The equilibrium structure in S_1 is aromatic (Fig.1 *a*). The transition between the three aromaticities may be induced either thermally or photochemically.[9,26,27] Geometric optimization was performed by starting with a boat-shaped or planar structure in all S_0 to S_3 states. We were unable to optimize the structure of COT (S_2) due to the small band gap with S_1 pointing to the lack of well-defined potential energy minimum (as detailed in SI). As shown in Fig.1 *a*, both of the D_{2d} symmetric boat-shaped minimum non-aromatic structures and the planar D_{4h} symmetric transition antiaromatic structures can be obtained by geometric optimization in S_0, with a slightly higher potential energy ($\Delta E = 0.5eV$) for the planar D_{4h} structure. The significant variances between the single and double bond length (listed in Fig.1 caption and references[28,29]) identified their aromaticity. For comparison, the native minimum S_1 structure has aromaticity with D_{8h} symmetry due to its planar geometry and a vanishing C-C bond length difference (0.005 Å). The band gaps are then analyzed based on the true boat-shaped S_0 optimal structure. Table. 1 compares the vertical excitation energies calculated by different methods. As being the case for other systems, semiempirical AM1/CIS results in red-shifted energies compared to time-dependent Density Functional Theory (TD-DFT) and *ab initio* CASSCF/CASPT2 methods. Importantly, the relaxation rates during the excited states dynamics are closely related to the energy gaps between states,[25] but not to the absolute values of the transition energies from the ground state. Therefore, the AM1/CIS approach is appropriate to conduct the COT NAMD simulation due to the good agreement of band-gaps with other higher-level

methods (e.g., TD-DFT and CASPT2).

Table 1: Comparison of the vertical excitation energies (in eV) for the first three singlet excited states of COT for different methods. TD-DFT simulations were performed with PBE0 functional and 6-31G* basis set.

Method	S_1	S_2	S_3
AM1/CIS	3.06	4.95	4.97
TD-DFT	3.61	5.34	5.35
CASSCF[8]	6.26	7.01	6.54
CASPT2[8]	4.00	5.75	6.00

Figure 1*b* shows the state transition density (TD) plotted for the first three singlet excited-states of COT evaluated at the boat-shape S_0 optimal geometry. The TD of S_1 state is evenly distributed on each C atom, while these quantities for S_2 and S_3 are disorderedly distributed around the nonplanar ring. Figure 1*c* shows the same excited-states TDs, however, based on the S_0 transition geometry. In the antiaromatic planar geometry, all three lowest electronic states exhibited an even TD distribution based on its symmetry around the ring. The antisymmetric structure of S_2 and S_3 TDs with respect to the horizontal and vertical planes, respectively, is pronounced. For comparison, the TDs of S_1 aromatic planar structure are also shown in Fig. 1*c*. D_{8h} COT has a pair of half-filled and degenerate non-bonding π orbitals[28] (i.e., delocalized π bond), in which the electrons freely move around the ring, as reflected by a broader S_2 and S_3 TD distributions in D_{8h} than D_{4h}.

To perform the NAMD simulations, we first conducted sampling of the initial conformational structures by running a 520 ps ground-state adiabatic molecular dynamics (AMD) trajectory of COT in vacuum using Langevin thermostat at 300 K with a timestep of 0.1 fs. Following a 20 ps equilibration period, 1000 snapshots of geometries and velocities were sampled every 0.5 ps as the initial conditions. The absorption spectrum analysis was preformed on those initial samples with a Gaussian lineshape and FWHM (full width at half-maximum) of 0.36 eV. The spectrum, shown in Fig. 1*e*, includes the contributions of the 8 lowest-energy excited states. The weakly absorbing S_1 feature (a tiny peak at 3.1 eV) reflects a forbidden S_0 to S_1 excitation (dark state). The higher-energy states $S_2 \sim S_8$ are optically bright

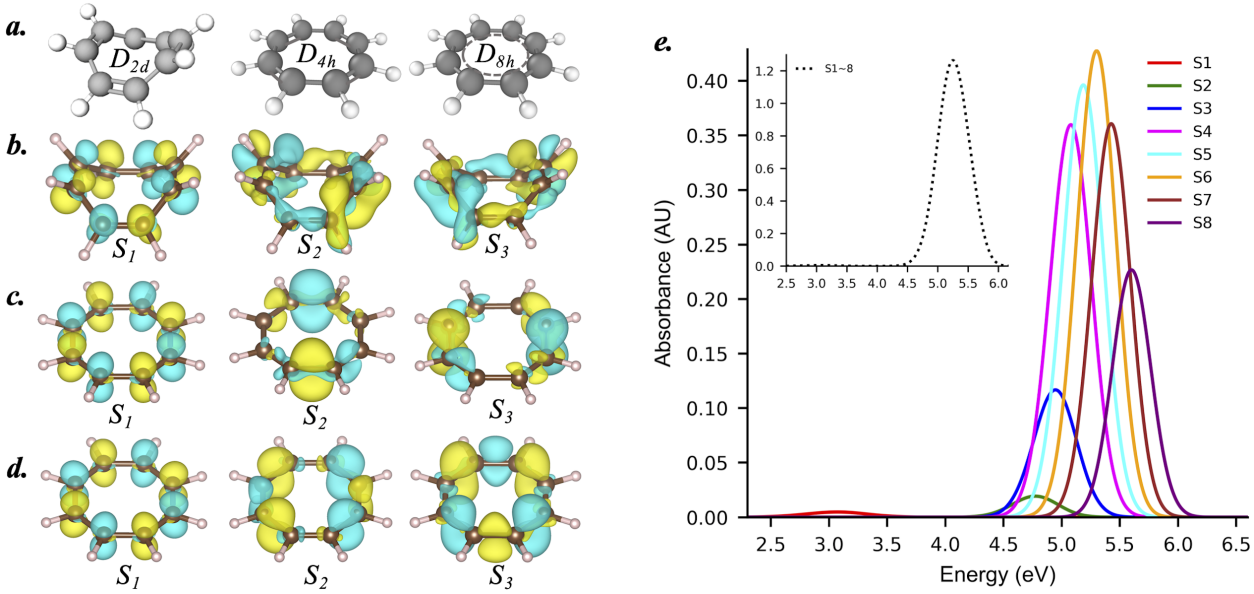

Figure 1: *a*. Ground state minimum geometry D_{2d} with bond lengths 1.344 Å $(C = C)$ and 1.479 Å $(C - C)$. Ground state transition (mata-stable) geometry D_{4h} with bond lengths 1.336 Å $(C = C)$ and 1.442 Å $(C - C)$. Native optimal S_1 geometry D_{8h} with equal $C - C$ bond lengths approximately $1.387 \sim 1.382$ Å. *b*. Orbital plots of the transition density (TD) for the lowest 3 electronic states at the ground state optimized geometry. *c*. The same but for the ground state transition geometry. *d*. The same but for the optimal S_1 geometry. *e*. Calculated absorption spectrum of COT at 300 K showing individual contributions of the 8 lowest excited electronic states. The insert shows the total absorption profile combining S_1 to S_8 contributions.

transitions forming a strong absorption band between 5.0 to 5.8 eV. These results are in a good agreement with early COT measurements in dye laser solution, which indicated an extremely weak absorption near 4.43 eV and intense spectrum around 5.5∼6.9 eV.[30,31]

The initial excited states were populated according to a Franck-Condon window $g_I(r, R) = f_I \exp[-T^2(E_{laser} - E_I)^2]$ where f_I and E_I are the oscillator strength and energy of excited state I, and E_{laser} is the energy of a Gaussian laser pulse $f(t) = \exp(-t^2/2T^2)$, centered at 5.0 eV that corresponds to the maximum of the absorption for the S_4 state (see Fig. 1e), with $T = 0.36$ eV for FWHM. The excited-state dynamics were then investigated using surface hopping NAMD in vacuum at 300K with a nuclear timestep of 0.025 fs and an electron timestep of 0.005 fs (see our previous NEXMD applications for more detail elsewhere[17–19]). Eight excited states were included in the simulations to allow for possible transitions to higher energy. The instantaneous decoherence correction and trivial unavoided crossings tracking were activated.

During NAMD, the overall non-radiative relaxation across trajectory ensemble can be monitored by tracking the evolution of the averaged adiabatic state populations, TD profile and COT geometry features. Figure 2a shows the quantum state populations[19] in NAMD simulation. According to the Franck-Condon window with 5.0 eV light impulse, the initially excited electronic states were concentrated around S_3 to S_6 band of states. About 50% of the trajectories relaxed back to the S_1 in 100 fs. After 400 fs, 90% of the trajectories have arrived to S_1. To monitor the spatial energy transfer, the averaged time-dependent localization of the electronic TD among different fractions[19] of the COT molecule was tracked across the 1000 trajectories in total as depicted in Fig. 2b. The transition density is evenly separated into two fractions (see the insert of Fig. 2b) on the ring, in which fragment F2 collected the TD contributions from C atoms 1, 2, 3, 4 and their bonding H atoms (refer to the insert Fig. 2e), and fragments F1 is the sum of TD from the rest of carbon atoms. Finally, Figures. 2$c \sim e$ plot the relevant geometric features (bond length, dihedral angle, and bond length alternation) monitoring the geometry evolution of COT in the NAMD process. The

selection of these parameters is detailed in SI.

As indicated by Garavelli et al.,[8,9] the photo-induced double-bond shifting mechanism included a transfer of localized π-bonds to form a delocalized aromatic π-system (Fig. 2 *a*) during the D_{2d} to D_{8h} structure transformation. Similar process is observed in our SH-NAMD simulations. As shown in Figs. 2 *b* and *c*, the D_{2d} structure has an uneven TD distribution in the $S_{n>1}$ states and a uniform TD distribution in S_1. Therefore, the strong TD fluctuation between F1 and F2 segments in the initial 150 fs of dynamics in Fig. 2*b* reflects an energy redistribution due to the fundamental π-bond transformation underpinning the double-bond shift. Meanwhile, a significant bond length oscillation shown in Fig. 2*e* was observed in the first 100 fs. Such oscillations in photoexcited molecular dynamics frequently signify appearance of coherent electronic-vibrational dynamics persisting across an ensemble of trajectories.[32] Finally, when the molecule relaxes to a D_8h aromatic structure (S_1), the localized π bonds overlap to form a delocalized aromatic π system across all C atoms of the ring. This explains the uniform TD distribution across fragments and diminishing bond length alternation when most of the trajectories were transferred to S_1 after 150 fs.

Internal conversion in molecular systems across a manifold of excited electronic states occurs on ultrafast timescales, typically below $\sim$1 ps.[33] In contrast, due to a large gap, nonradiative transitions back to the ground state usually happen on much longer (tens of ps to nanosecond) timescales. Here, barrierless ultrafast photoisomerisations such as rhodopsin dynamics[7] are notable exceptions. Description of non-Born-Oppenheimer transitions to the ground state have inherent multireference character and can cannot be properly described with a single-reference methods such as Hartree-Fock or DFT. For example, as mentioned in other published works,[34,35] conical intersections between the ground and excited state in the latter methods have incorrect dimensionality owing to the Brillouin theorem.[36,37] This calls for the use of alternative approaches.[22,38] In a previous study,[39] we introduce a simple "Open-GS" method[33,40] to treat such transitions to the ground state: when the system is in the lowest energy excited state and the energy gap between ground and excited state ($\Delta E_{S_{0-1}}$)

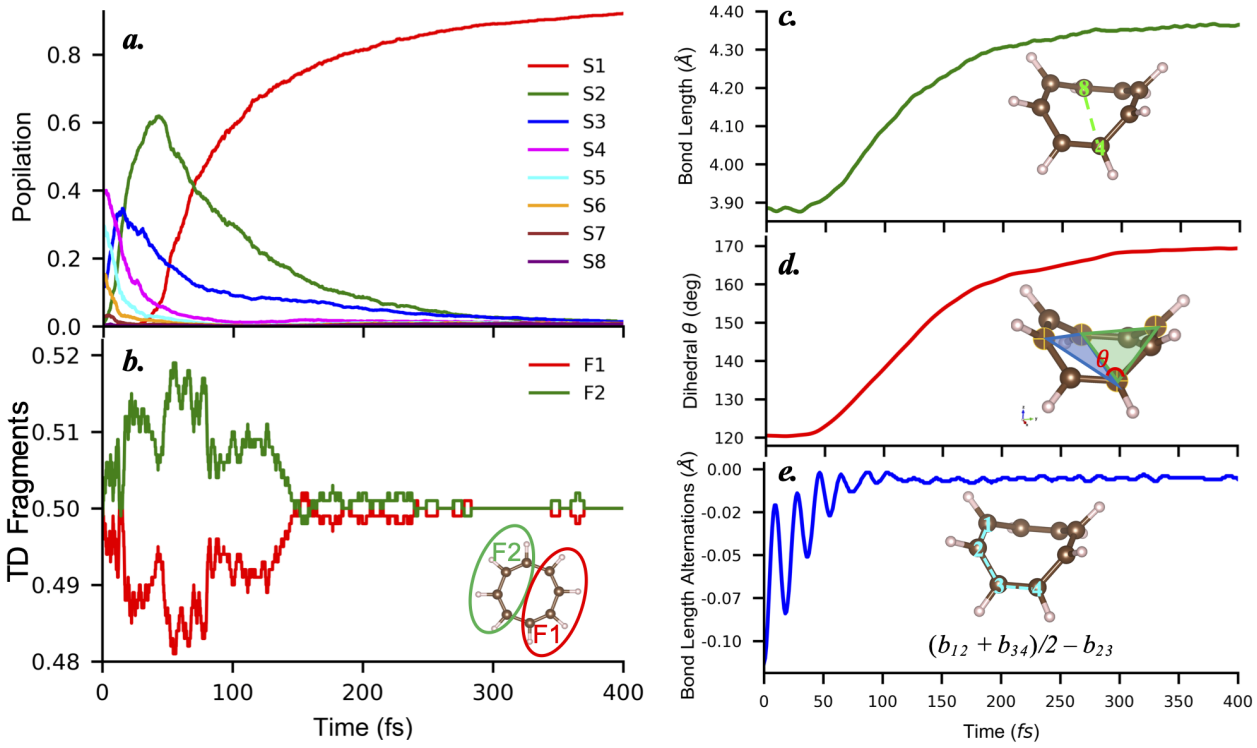

Figure 2: *a*. Average populations of S_1 to S_8 electronic states as a function of time from NAMD simulations. *b*. Electronic transition density localized on each molecular fragment averaged over all trajectories. *c*. Plot of the bond length b_{48} over time. *d*. Plot of the dihedral angle θ over time. *e*. Plot of the bond length alternations $(b_{12}+b_{34})/2-b_{23}$ over time.

is smaller than a certain threshold (normal 0.5 eV), the non-adiabatic transition is enforced, and the dynamics continues on the ground state potential energy surface (PES). Indeed, the $\Delta E_{S_{0-1}}$ energy gap is becoming small in COT molecule (see SI) once the trajectory approaches the S_1/S_0 conical intersection seam. We set a threshold $\Delta E_{S_{0-1}} = 0.1$ eV to enforce the transition from S_1 to S_0 state with an excess of electronic energy redistributed into nuclear kinetic energy.[41,42] Accordingly, to model the final phase of COT photoinduced dynamics (i.e., S_1/S_0 transition), we selected 300 configurations from NAMD, which have stabilized in S_1 state for 10 fs without hopping upward to S_2 as the initial conditions for the adiabatic molecular dynamics (AMD) simulation in S_1 state at 300 K. As this dynamics progressed, 291 terminated trajectories (out of 300 total) reached S_1/S_0 conical intersection seam within 20 ps of S_1 AMD. These trajectories were then re-initiated at S_0 state.

Figures 3*a* to *d* plot the geometric features and energy profile for a typical trajectory in S_1 AMD simulation. The trajectory sampling S_1 PES in Fig. 3*c* indicates that it traverses an energy barrier ($\sim$0.3 eV) before reaching the S_1/S_0 conical intersection. When crossing the barrier at 3.2 ps, a slight folding of the D_{8h} planar structure is detected, which is reflected as the valleys in the dihedral angle and average bond length plot (Figs. 3*a* and *b*). By combining the geometric features with the $\Delta E_{S_{0-1}}$ energy gaps shown in Fig. 3*d*, we conclude that the folding deformation of the planar structure is accompanied by an increase of the $\Delta E_{S_{0-1}}$ is observed near the barrier (3.2 ps and 6 ps points). The results clearly show that after crossing the energy barrier, the folded S_1 structure needs to convert back to a less folded conformation to be able to reach the S_1/S_0 conical intersection. Compared to Ref.,[8] the "planar-like" CI structure observed in our AMD simulations is somewhere on between previously suggested folded (quasi-tetraradical, CI_b) and (triangular -$(CH)_3$- kink as (CI_{st}). We believe that such intermediate structures appear due to thermal effects in AMD, where trajectories reach the extended S_1/S_0 crossing seam at different conical intersection conformations, eventually producing crossing points with intermediate structures with respect to the two extreme points located by the minimized energy paths presented in (Ref.[8]). Finally, the S_1 AMD

simulation is terminated once the $\Delta E_{S_{0-1}}$ gets below 0.1 eV (Fig. 3*d*).

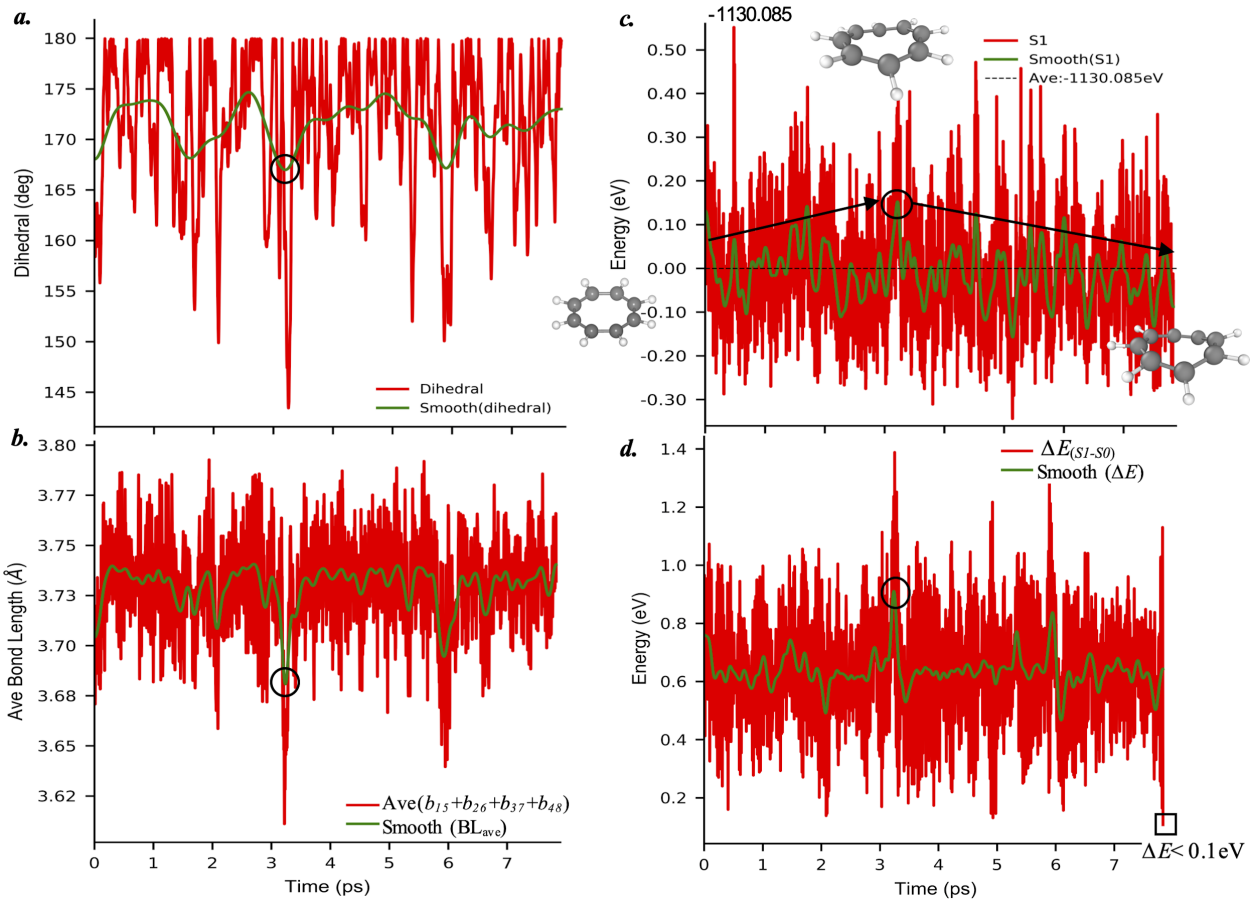

Figure 3: Analysis of a typical AMD trajectory on S_1 state. Plots of the dihedral angle (a), the average bond lengths (b_{15}, b_{48}, b_{37} and b_{48}) between all diagonal atoms (b), the total S_1 state energy referenced with respect to its average -1130.085 eV (c), and the $\Delta E_{S_{0-1}}$ energy gap (d) with time. The green line in each plot is an average using Savitzky-Golay filter[43] for every 100 data points.

Similar energy barrier crossing features were observed in all S_1 AMD simulations, however, the S_1 AMD trajectory lengths varied significantly. Compared to the $S_{n>1}$ to S_1 relaxation occuring within ~400 fs, the S_1 to S_0 transition appears between 1 to 12 ps. In some extreme cases ($< 10\%$), the trajectory can stay on S_1 for over 20 ps. Figure 4*a* shows the total excitation lifetime distribution of $S1$. The peaks around 1.6 ps of the histogram plot indicated the possible excitation lifetime of COT before reaching S_1/S_0 crossing.

Finally, we collected the S_1/S_0 crossing crossing configurations sampled from S_1 AMD simulations, when the gap $\Delta E_{S_{0-1}}$ becomes smaller then 0.1 eV. These AMD trajectories

were continued on the ground state S_0 potential energy surface at 300 K (i.e. transition to the ground state were enforced) with excess of energy ($\Delta E_{S_{0-1}}$) being dispersed in nuclear kinetic energy. In this way, the photoproduct of COT is connected with the thermal reaction paths that include the S_0 potential energy surface. As a comparison, pure thermal reaction channel simulations were also initiated on S_0 from a ground state optimized D_{2d} boat-shape and planar D_{4h} COT structures, respectively. Figure 4*b* shows the time dependent energy profiles of both D_{2d} and D_{4h} thermal reaction dynamics on S_0: it takes around 0.2 ps for the system to reach the target temperature (300 K), then the plots demonstrate that the planar D_{4h} COT ultimately equilibrates to a D_{2d} boat-shaped structure by crossing an energy barrier. As shown in Fig. 4*c*, the S_0 AMD starting from the S_1/S_0 conical intersection structure exhibits a coinciding equilibration progress as the thermal reaction path of the planar D_{4h} structure, and the structure at the observed barrier from the thermal reaction MD is similar to the S_1/S_0 crossing points where the excited state branches of the MD are terminated. This establishes the connection between the S_1/S_0 crossing structure and the continuous S_0 simulations for thermal reaction channel, and further clarifies the final phase of COT in the ground state dynamics toward equilibrium boat-shaped geometry.

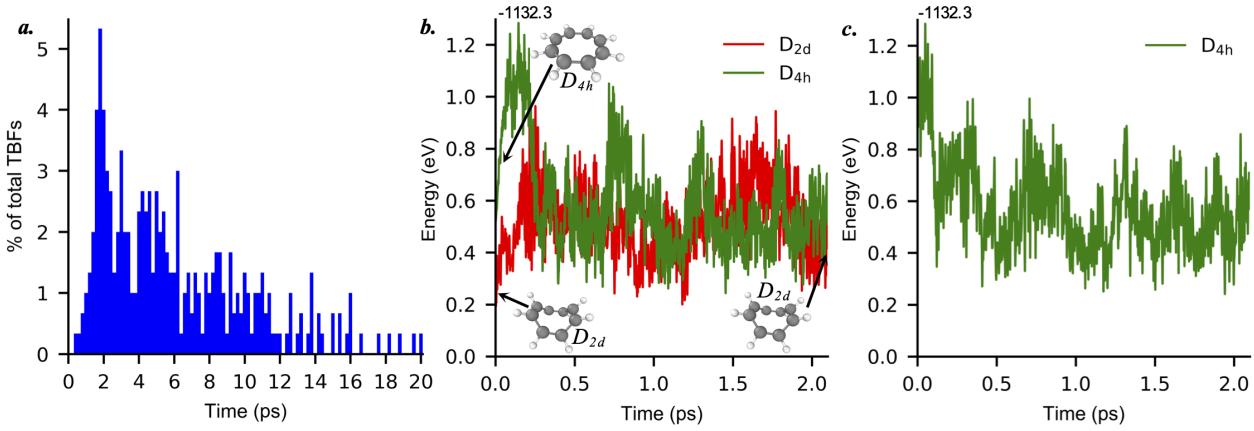

Figure 4: *a*. is the distribution of timescales for photoexcited COT before reaching S_1/S_0 conical intersection. *b*. and *c*. analysis of representative S_0 AMD trajectories started from different conditions at 300 K. *b*. two trajectories initiated from D_{2d} boat-shape and planar D_{4h} COT structures . The inserts show the initial and final COT geometries. *c*. a trajectory initiated from the S_1/S_0 transition structure. *b* and *c* plots are referenced to the ground state potential energy minimum -1132.3 eV.

In summary, our dynamical simulations provide a comprehensive map of excited-state relaxation pathways in the photoexcited cyclooctatetraene. We used our NEXMD software to perform the non-adiabatic molecular dynamics simulation ($S_{n>1}$ to S_1 states) and adiabatic molecular dynamics simulation (at S_1 and S_0 states) of COT at ambient conditions. An active excited to ground state relaxation pathway accompanied with a complete double-bond shifting progress of COT, was determined as follows: boat-shaped D_{2d} structure ($S_{n>1}$) $\rightarrow$ planar D_{8h} structure (S_1) $\rightarrow$ slightly folded S_1 meta-stable structure $\rightarrow$ planer D_{4h} at S_1/S_0 conical intersection $\rightarrow$ boat-shaped D_{2d} ground state equilibrium structure. Determined structural changes agree well with those determined from the high level *ab initio* simulations. Moreover, the excitation lifetime obtained from our molecular dynamics simulation shows an excellent agreement with the experimental measurements. Our detailed dynamical results can thus provide a fundamental basis for further investigating the bond order inversion and photo-switching process in the COT molecular systems.

Supporting Information

Supporting Information provides: S1. Potential Energy Analysis; S2. Geometric Features Analysis.

Acknowledgement

H.S., S.T., and S.M. acknowledge support from the U.S. Department of Energy, Office of Science, Basic Energy Sciences, Chemical Sciences, Geosciences, and Biosciences Division under Contracts No. KC0301030, KC030103172684, and award No. DE-SC0019484. H.S. and S.T. acknowledges support of the Center for Integrated Nanotechnology (CINT) at Los Alamos National Laboratory (LANL), a U.S. Department of Energy and Office of Basic Energy Sciences User Facility. This research used resources provided by the LANL Institutional Computing Program. D. K. gratefully acknowledges support from the Alexander von

Humboldt Foundation through the Feodor Lynen program.

References

(1) Briquet, A. A. S.; Uebelhart, P.; Hansen, H.-J. Double-Bond Shifts in [4n]Annulenes as a New Principle for Molecular Switches: First Results with Dimethyl Heptalene-1,2- and -4,5-dicarboxylates. *Helvetica Chimica Acta* **1996**, *79*, 2282–15.

(2) Aprahamian, I. The Future of Molecular Machines. *ACS Central Science* **2020**, *6*, 347–358.

(3) Zimmerman, H. E.; Iwamura, H. Thermal and photochemical interconversions of cyclooctatetraenes and semibullvalenes. Exploratory organic photochemistry. LII. *J. Am Chem. Soc.* **1970**, *92*, 2015–22.

(4) Sekkat, Z. In *Photoreactive Organic Thin Films*; Sekkat, Z., Knoll, W., Eds.; Academic Press: San Diego, 2002; pp 271–287.

(5) Neukirch, A. J.; Shamberger, L. C.; Abad, E.; Haycock, B. J.; Wang, H.; Ortega, J.; Prezhdo, O. V.; Lewis, J. P. Nonadiabatic ensemble simulations of cis-stilbene and cis-azobenzene photoisomerization. *J. Chem. Theory Comput.* **2014**, *10*, 14–23.

(6) Kandori, H.; Shichida, Y.; Yoshizawa, T. Photoisomerization in Rhodopsin. *Biochemistry (Moscow)* **2001**, *66*, 1197–1209.

(7) Suomivuori, C.-M.; Gamiz-Hernandez, A. P.; Sundholm, D.; Kaila, V. R. I. Energetics and dynamics of a light-driven sodium-pumping rhodopsin. *Proceedings of the National Academy of Sciences* **2017**, *114*, 7043–48.

(8) Garavelli, M.; Bernardi, F.; Cembran, A.; Castaño, O.; Frutos, L. M.; Merchán, M.; Olivucci, M. Cyclooctatetraene Computational Photo- and Thermal Chemistry: A Reactivity Model for Conjugated Hydrocarbons. *J. Am. Chem. Soc.* **2002**, *124*, 13770–89.

(9) Garavelli, M.; Bernardi, F.; Moliner, V.; Olivucci, M. Intrinsically Competitive Photoinduced Polycyclization and Double-Bond Shift through a Boatlike Conical Intersection. *Angew. Chem. Int. Ed.* **2001**, *40*, 1466–68.

(10) Tokizaki, C.; Yoshida, T.; Takayanagi, T. Theoretical analyses of the time-resolved nuclear dynamics of the transition state for the 1,3,5,7-cyclooctatetraene unimolecular reaction. *Comput. Theor. Chem.* **2017**, *1112*, 20–26.

(11) Chang, J.-L.; Cheng, M.-Z.; Huang, Y.-J. Theoretical Study of the Negative Ion Photoelectron Spectrum of Cyclooctatetraene via Computation of Franck–Condon Factors. *J. Phys. Chem. A.* **2020**, *124*, 3205–13.

(12) Yoshida, T.; Tokizaki, C.; Takayanagi, T. Theoretical analysis of the transition-state spectrum of the cyclooctatetraene unimolecular reaction: Three degree-of-freedom model calculations. *Chem. Phys. Lett.* **2015**, *634*, 134–139.

(13) Tokizaki, C.; Yoshida, T.; Takayanagi, T. Quantum Transition State Dynamics of the Cyclooctatetraene Unimolecular Reaction on Ab Initio Potential Energy Surfaces. *Chem. Phys.* **2016**, *469-470*, 97–104.

(14) Tully, J. C. Molecular Dynamics with Electronic Transitions. *J. Chem. Phys.* **1990**, *93*, 1061–1071.

(15) Nelson, T.; Fernandez-Alberti, S.; Roitberg, A.; Tretiak, S. Nonadiabatic excited-state molecular dynamics: Treatment of electronic decoherence. *J. Chem. Phys.* **2013**, *138*, 224111–224124.

(16) Fernandez-Alberti, S.; Roitberg, A. E.; Nelson, T.; Tretiak, S. Identification of unavoided crossings in nonadiabatic photoexcited dynamics involving multiple electronic states in polyatomic conjugated molecules. *J. Chem. Phys.* **2012**, *137*, 14512–14522.

(17) Nelson, T.; Fernandez-Alberti, S.; Chernyak, V.; Roitberg, A.; Tretiak, S. Nonadiabatic Excited-State Molecular Dynamics Modeling of Photoinduced Dynamics in Conjugated Molecules. *J. Phys. Chem. B* **2011**, *115*, 5402–5414.

(18) Nelson, T.; Fernandez-Alberti, S.; Roitberg, A.; Tretiak, S. Nonadiabatic Excited-State Molecular Dynamics: Modeling Photophysics in Organic Conjugated Materials. *Acc. Chem. Res.* **2014**, *47*, 1155–1164.

(19) Malone, W.; Nebgen, B.; White, A.; Zhang, Y.; Song, H.; Bjorgaard, J.; Sifain, A.; Rodriguez-Hernandez, B.; Freixas, V.; Fernandez-Alberti, S.; Roitberg, E.; Nelson, R.; Tretiak, S. NEXMD Software Package for Non-adiabatic Excited State Molecular Dynamics Simulations. *J. Chem. Theory Comput* **2020**, *16*.

(20) Tretiak, S.; Zhang, W. M.; Chernyak, V.; Mukamel, S. Excitonic couplings and electronic coherence in bridged naphthalene dimers. *Proc. Nat. Acad. Sci.* **1999**, *96*, 13003–13008.

(21) Stewart, J. J. P. Optimization of Parameters for Semiempirical Methods IV: Extension of MNDO, AM1, and PM3 to More Main Group Elements. *J. Mol. Model.* **2004**, *10*, 155–64.

(22) Li, S. L.; Marenich, A. V.; Xu, X.; Truhlar, D. G. Configuration Interaction-Corrected Tamm–Dancoff Approximation: A Time-Dependent Density Functional Method with the Correct Dimensionality of Conical Intersections. *The journal of physical chemistry letters* **2014**, *5*, 322–328.

(23) Nelson, T. R.; White, A. J.; Bjorgaard, J. A.; Sifain, A. E.; Zhang, Y.; Nebgen, B.; Fernandez-Alberti, S.; Mozyrsky, D.; Roitberg, A. E.; Tretiak, S. Non-adiabatic Excited-State Molecular Dynamics: Theory and Applications for Modeling Photophysics in Extended Molecular Materials. *Chem. Rev.* **2020**, *120*, 2215–87.

(24) Zheng, F.; Fernandez-Alberti, S.; Tretiak, S.; Zhao, Y. Photoinduced Intra- and Intermolecular Energy Transfer in Chlorophyll a Dimer. *The Journal of Physical Chemistry B* **2017**, *121*, 5331–39.

(25) Mukazhanova, A.; Malone, W.; Negrin-Yuvero, H.; Fernandez-Alberti, S.; Tretiak, S.; Sharifzadeh, S. Photoexcitation dynamics in perylene diimide dimers. *J. Chem. Phys.* **2020**, *153*, 244117.

(26) Stevenson, C. D.; Brown, E. C.; Hrovat, D. A.; Borden, W. T. Isotope Effects on the Ring Inversion of Cyclooctatetraene. *J. Am. Chem. Soc.* **1998**, *120*, 8864–67.

(27) Paquette, L. A. The current view of dynamic change within cyclooctatetraenes. *Acc. Chem. Res.* **1993**, *26*, 57–62.

(28) Nishinaga, T.; Ohmae, T.; Iyoda, M. Recent Studies on the Aromaticity and Antiaromaticity of Planar Cyclooctatetraene. *Symmetry* **2010**, *2*, 76–97.

(29) Gellini, C.; Salvi, P. R. Structures of Annulenes and Model Annulene Systems in the Ground and Lowest Excited States. *Symmetry* **2010**, *2*, 1846–24.

(30) Palmer, M. H.; Hoffmann, S. V.; Jones, N. C.; Coreno, M.; de Simone, M.; Grazioli, C. The electronically excited states of cyclooctatetraene—An analysis of the vacuum ultraviolet absorption spectrum by ab initio configuration interaction methods. *J. Chem. Phys.* **2019**, *151*, 084304.

(31) Frueholz, R. P.; Kuppermann, A. Electronic spectroscopy of 1,3,5,7-cyclooctatetraene by low-energy, variable-angle electron impact. *J. Chem. Phys.* **1978**, *69*, 3614–21.

(32) Kobayashi, Y.; Chang, K. F.; Poullain, S. M.; Scutelnic, V.; Zeng, T.; Neumark, D. M.; Leone, S. R. Coherent electronic-vibrational dynamics in deuterium bromide probed via attosecond transient-absorption spectroscopy. *Phys. Rev. A* **2020**, *101*, 063414.

(33) Parker, S.; Rappoport, D.; Furche, F. Quadratic Response Properties from TDDFT: Trials and Tribulations. *Phys. Chem. Chem. Phys.* **2019**, *21*, 18999–19010.

(34) Parker, S.; Roy, S.; Furche, F. Multistate hybrid time-dependent density functional theory with surface hopping accurately captures ultrafast thymine photodeactivation. *J. Chem. Theory. Comput.* **2018**, *14*, 807–819.

(35) Stojanović, L.; Bai, S.; Nagesh, J.; Izmaylov, A. F.; Crespo-Otero, R.; Lischka, H.; Barbatti, M. New Insights into the State Trapping of UV-Excited Thymine. *Molecules* **2016**, *21*, 1603.

(36) Szabo, A.; Ostlund, N. S. *Modern quantum chemistry: introduction to advanced electronic structure theory*; Courier Corporation, 2012.

(37) Levine, B. G.; Ko, C.; Quenneville, J.; Martnez, T. J. Conical intersections and double excitations in time-dependent density functional theory. *Mol. Phys.* **2006**, *104*, 1039–1051.

(38) Tapavicza, E.; Bellchambers, G. D.; Vincent, J. C.; Furche, F. *Ab Initio* non-adiabatic molecular dynamics. *Phys. Chem. Chem. Phys.* **2013**, *15*, 18336–18348.

(39) Zhang, Y.; Mukamel, S.; Khalil, M.; Govind, N. Simulating Valence-to-Core X-ray Emission Spectroscopy of Transition Metal Complexes with Time-Dependent Density Functional Theory. *JCTC* **2015**, *11*, 5804–5809.

(40) Furche, F.; Perdew, J. P. The performance of semilocal and hybrid density functionals in 3d transition-metal chemistry. *J. Chem. Phys.* **2006**, *124*, 044103.

(41) Fabiano, E.; Keal, T. W.; Thiel, W. Implementation of surface hopping molecular dynamics using semiempirical methods. *Chem. Phys.* **2008**, *349*, 334–437.

(42) Song, H.; Fischer, S. A.; Zhang, Y.; Cramer, C. J.; Mukamel, S.; Govind, N.; Tretiak, S. First Principles Nonadiabatic Excited-State Molecular Dynamics in NWChem. *J. Chem. Theory Comput* **2020**, *16*.

(43) Savitzky, A. A Historic Collaboration. *Analytical Chemistry* **1989**, *61*, 921A–23A.